

NASA Contractor Report 187524

1N-02

8218

817

(NASA-CR-187524) AERODYNAMIC PARAMETER
STUDIES AND SENSITIVITY ANALYSIS FOR ROTOR
BLADES IN AXIAL FLIGHT (Lockheed
Engineering and Sciences Corp.) 17 p

N91-22078

CSSL 01A G3/02

Unclas
0008218

**AERODYNAMIC PARAMETER STUDIES
AND SENSITIVITY ANALYSIS FOR
ROTOR BLADES IN AXIAL FLIGHT**

Y. Danny Chiu

**LOCKHEED ENGINEERING & SCIENCES COMPANY
Hampton, Virginia**

David A. Peters

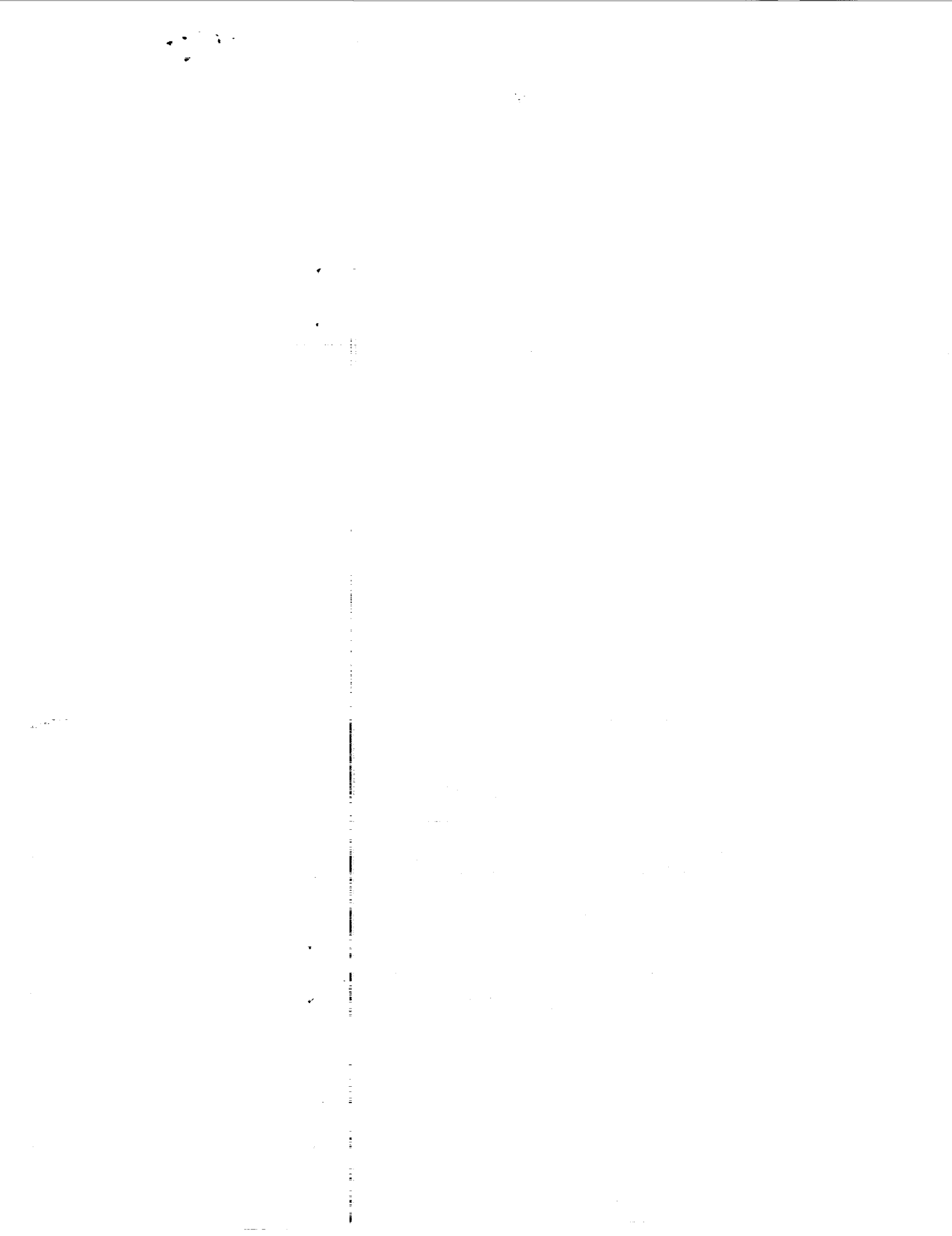
**GEORGIA INSTITUTE OF TECHNOLOGY
Atlanta, Georgia**

**Contract NAS1-19000
Grant NAG1-710
March 1991**

NASA

National Aeronautics and
Space Administration

Langley Research Center
Hampton, Virginia 23665-5225



AERODYNAMIC PARAMETRIC STUDIES AND SENSITIVITY ANALYSIS FOR ROTOR BLADES IN AXIAL FLIGHT

Y. Danny Chiu
Research Engineer
Lockheed Engineering and Science Company
Hampton, Virginia 23666

David A. Peters
Professor
School of Aerospace Engineering
Georgia Institute of Technology
Atlanta, Georgia 30332

Abstract

This paper offers analytical capability for aerodynamic parametric studies and sensitivity analysis of rotary wings in axial flight by using a 3-dimensional undistorted wake model in curved lifting-line theory. The governing equations are solved by both the Multhopp Interpolation technique and the Vortex Lattice method. The singularity from the bound vortices is eliminated through the Hadamard's finite part concept. Good numerical agreement between both analytical methods and finite difference methods are found. Parametric studies were made to assess the effects of several shape variables on aerodynamic loads. It is found, for example, that a rotor blade with out-of-plane and inplane curvature can theoretically increase lift in the inboard and outboard regions respectively without introducing an additional induced drag.

Notation

<p>AR aspect ratio, R / c_e</p> <p>a lift curve slope, $\approx 2\pi$</p> <p>b number of blades</p> <p>c chord length</p> <p>c_o chord length at blade root</p> <p>c_1 chord length at blade tip</p> <p>c_e equivalent chord</p> <p>\bar{c} $c(x)/c_o$</p> <p>C_L total lift coefficient</p> <p>C_{D_i} total induced drag coefficient</p> <p>C_{P_i} total induced power coefficient</p> <p>K coefficient factor, c_e / c_o</p> <p>M number of terms in Multhopp Interpolation Technique or number of panels in VLM</p> <p>m summation integer; also weighting factor index</p> <p>p tip shape parameter</p> <p>R rotor radius</p>	<p>r radial distance</p> <p>S_R area of a rotor in X-Y plane, $=R c_e$</p> <p>x, y, z normalized coordinates with respect to R</p> <p>β tip length parameter</p> <p>δ twist shape parameter; also $\tan^{-1}(\epsilon\eta)$</p> <p>ϵ inplane curvature</p> <p>θ twist angle</p> <p>$\bar{\theta}(r)$ $\theta(x)/\theta_o$</p> <p>θ_o twist angle at blade root</p> <p>θ_1 twist angle at blade tip</p> <p>κ out-of-plane curvature</p> <p>η dummy variable representing spanwise distance</p> <p>λ taper ratio, c_1/c_o</p> <p>ρ air density</p> <p>σ rotor solidity, $bc_e/\pi R$</p> <p>τ twist ratio, θ_1/θ_o</p> <p>v inflow ratio, $=v_i + v_c/\theta_o$</p> <p>v_c climb inflow ratio, $V_{climb}/R \Omega$</p> <p>v_i induced inflow ratio, $v_L + v_T$</p> <p>v_L induced inflow ratio from curved lifting-line</p> <p>v_T induced inflow ratio from trailing vortex lines</p> <p>ζ $\tan^{-1}(\epsilon x)$</p> <p>ψ azimuthal angle; also Digamma function</p> <p>Γ circulation; also Gamma function</p> <p>$\bar{\Gamma}$ normalized circulation, $\Gamma/R^2\Omega\theta_o$</p> <p>Ω angular velocity</p>
---	--

Introduction

A key ingredient in developing reliable and efficient procedures for design optimization of aerospace structures is sensitivity analysis. This is especially true for aerodynamic sensitivity analysis which is of growing importance for aerodynamic shape optimization as well as the interdisciplinary process of integrating aerodynamics with other disciplines. A recent paper by Sobieski¹ stresses the need for aerodynamic sensitivity analysis and

makes a plea to the aerodynamic community for extending their present capability to include sensitivity analysis. The present paper attempts to partially fill this void for the rotary wings.

In recent years there has been a resurgence of interest in the idea of reducing the induced drag of an aircraft by wing design. Some examples of recent work suggest the use of inplane²⁻⁴ or out-of-plane⁵ curvature. There have been few attempts to extend this idea to rotary wings. The present paper is intended to establish sensitivity analysis for rotor blades in axial flight.

In previous work, Rand and Rosen⁶ developed a lifting line model which is capable of calculating the aerodynamic load along inplane curved-blades of a helicopter in hovering and axial flight. Their method, however, should be classified as the Vortex Lattice Method (VLM) and is an approximate approach to solve the singular integro-differential equation. The present paper deals with the same problem by using an analytical approach to solve the more general governing equation which can include the analysis of out-of-plane curved blades. The analytical approach, in the present paper, uses the Multhopp Interpolation technique which is a special case of Fourier Series method and widely used in fixed-wing cases for both lifting-line⁷ and lifting-surface^{8,9} models. As mentioned in Ref. 6, the difficulty, raised in the case of inplane curved blades, is the fact that the velocity which is induced on the lifting line by the bound vortex itself obtains infinite values. This phenomenon is due to the singularity of the order $1/|x|$ which occurs in the development. This singularity may be handled elegantly by the Hadamard's finite part concept¹⁰ as described in Ref. 11. In this paper, we apply a similar technique to eliminate the singularity.

This paper also contains parametric studies which can quickly assess the effects of several shape variables on aerodynamic loads. The design variables are taper ratio, tip length, tip shape, aspect ratio, inplane curvature, out-of-plane curvature, twist ratio, and twist shape. Most rotor blades may be described by these shape parameters. Aerodynamic functions are local circulation, local induced velocity, total lift coefficient, total induced drag coefficient, lift-drag ratio, and induced power coefficient. The rotor performance is strongly dependent on these aerodynamic functions.

Aerodynamic Functions and Shape Design Variables.

The present paper deals with a rotor system having b identical, equally spaced blades. These blades rotate about the shaft with a constant angular velocity Ω . The rotor in Figs. 1 and 2, has a radius R and no hinge offset. The steady lifting-line theory, based on the three-dimensional undistorted wake model, will be applied to cases for

which helicopter rotors or propellers are in axial flight (including hovering). The shape design variables characterize three essential parameters of a blade: lifting-line shape, chord distribution, and twist distribution. The design variables are taper ratio, tip length, tip shape, aspect ratio, inplane curvature, out-of-plane curvature, twist ratio, and twist shape. Aerodynamic functions are local circulation, local induced velocity, total lift coefficient, total induced drag coefficient, lift-drag ratio, and induced power coefficient. Further details of the shape design variables are given next.

Lifting line shape

The reference blade in Figs. 1 and 2 is positioned at the 90 degree azimuthal angle. The origin or center of rotation is on the blade root one quarter-chord away from the leading edge. The inplane position y , and out-of-plane position z , of the lifting-line are assumed to have the form:

$$y = f(x) = \epsilon x^2 ; z = g(x) = \kappa x^2$$

where x is the spanwise direction, ϵ is the inplane curvature, and κ is the out-of-plane curvature. All quantities are normalized with respect to blade radius, R . When ϵ , and κ are equal to zero, it is a straight lifting-line. The rotor blade can have either backward inplane curvature ($\epsilon > 0$) or forward inplane curvature ($\epsilon < 0$) and have either upward curvature ($\kappa < 0$) or downward curvature ($\kappa > 0$). Also, we assume that $|\epsilon|$, and $|\kappa|$ are smaller than 0.3 so that the lifting-line theory remains valid.

Chord distribution:

The chord length $\bar{c}(x)$ normalized with respect to root chord has the following variation along the spanwise direction :

$$\bar{c}(x) = \frac{c(x)}{c_o} = [1 + x(\lambda - 1)][1 - x^{1/\beta}]^p$$

where λ is the taper ratio and is defined as the ratio of tip chord c_1 to root chord c_o , shown in Fig. 2. Note that we define λ as the inverse of conventional taper ratio. When λ is equal to 0, the blade is triangular.

The tip shape parameter is denoted p and is always positive. The physical meaning of p is to define the tip shape of a blade as shown in Fig. 3. The tip length parameter is denoted β and is also positive. The physical meaning of β is to define the extent of the tip taper as shown in Fig. 4. In general, all cases of chord distribution can be defined on the combinations of these three parameters.

Another important design variable is the solidity σ , (or the aspect ratio AR), which is defined as:

$$\sigma = \frac{bc_e}{\pi R} = \frac{b}{\pi(AR)}$$

where b is the number of blades, AR is the aspect ratio, and c_e is the equivalent chord, which is based on the equivalent thrust generated by the reference rotor with a rectangular planform, and has the following form:

$$c_e = \frac{\int_0^1 x^m c(x) dx}{\int_0^1 x^m dx} = K(m, \lambda, \beta, p) c_o$$

where m is the weighting factor index and is dependent on design criteria, such as blade area or area, thrust, or torque weighted solidity. Once m , β , p and λ are specified for a rotor, K can be analytically expressed in terms of the Gamma function as :

$$K = K_1 + (\lambda - 1) K_2$$

where

$$K_1 = \frac{(m+1) \beta \Gamma(p+1) \Gamma(\beta + m\beta)}{\Gamma(p+1+\beta + m\beta)}$$

$$K_2 = \frac{(m+1) \beta \Gamma(p+1) \Gamma(2\beta + m\beta)}{\Gamma(p+1+2\beta + m\beta)}$$

In order to calculate sensitivity derivatives, it is necessary to derive $\partial K / \partial \lambda$, $\partial K / \partial p$, and $\partial K / \partial \beta$, which are analytically expressed in terms of the Gamma and Digamma functions as Γ and ψ respectively:

$$\frac{\partial K}{\partial \lambda} = K_2$$

$$\frac{\partial K}{\partial p} = K_1 [\psi(p+1) - \psi(p+1+\beta + m\beta)]$$

$$+ (\lambda - 1) K_2 [\psi(p+1) - \psi(p+1+2\beta + m\beta)]$$

$$\frac{\partial K}{\partial \beta} = K_1 \left[\frac{1}{\beta} + (m+1) \psi(\beta + m\beta) - (m+1) \psi(p+1+\beta + m\beta) \right]$$

$$+ (\lambda - 1) K_2 \left[\frac{1}{\beta} + (m+2) \psi(2\beta + m\beta) - (m+2) \psi(p+1+2\beta + m\beta) \right]$$

Twist distribution:

The normalized twist angle of attack $\bar{\theta}(x)$ with respect to twist angle at blade root along the spanwise direction is defined in the following form:

$$\bar{\theta}(x) = \frac{\theta(x)}{\theta_o} = 1 + x^\delta (\tau - 1)$$

where τ is the twist ratio, defined as the ratio of tip twist θ_1 to root twist θ_o . δ is the twist shape parameter and is always positive. The physical meaning of τ is to define the twist distribution along a blade as shown in Fig. 5. The reason behind this τ definition is that an ideally twisted blade can be approximately modelled by concave twist (i.e., $0 < \tau < 1$). In order to calculate sensitivity derivatives, it is necessary to derive $\partial \bar{\theta} / \partial \tau$, and $\partial \bar{\theta} / \partial \delta$ which are expressed as:

$$\frac{\partial \bar{\theta}(x)}{\partial \tau} = x^\delta$$

$$\frac{\partial \bar{\theta}(x)}{\partial \delta} = \ln(x) x^\delta (\tau - 1)$$

Theoretical Derivations

Governing equation for circulation:

To derive the governing equation for circulation, we assume that the flow field is incompressible. Each blade is represented by a curved lifting line. The circulation along each lifting line is $\Gamma(r)$. Since Γ varies along the blade, vortex filaments must trail behind the rotating blade by $d\Gamma/dr$. It is further assumed that the trailing vortex system is an undistorted wake and moves downward with a climb velocity, V_{climb} , which is equal to the sum of the rotor axial velocity and the averaged induced-velocity around the rotor disk. The derivation follows similar derivations which have been developed in Refs. 12-13. However, an additional term of downwash due to the self-induced velocity from the bound vortex of lifting line has to be included. A similar study for fixed-wing cases can be found in Ref. 14. The governing equation used to solve for local circulation, $\bar{\Gamma}$, is very similar to those contained in other references. See for example, Ref. 6, Eq. (34) or Ref. 15, Eq. (3.17). It is the integro-differential equation which has the following form:

$$\frac{\sigma a}{2K} \bar{c}(x) [x \bar{\theta}(x) - v(x)] = \frac{b}{\pi} \bar{\Gamma}(x) \quad (1)$$

where

$$v(x) = v_i(x) + \frac{v_c}{\theta_o}; \quad v_i(x) = v_L(x) + v_T(x);$$

$$\sigma = \frac{b}{\pi AR} = \frac{bc_e}{\pi R} = \frac{Kbc_o}{\pi R}; \quad \bar{\Gamma}(x) = \frac{\Gamma(r)}{R^2 \Omega \theta_o}$$

here, a is the lift slope $\approx 2\pi$ and v_c is the climb inflow ratios. v_T and v_L are the induced inflow ratios, contributed by the curved lifting-line and trailing vortex lines, and can be derived by Biot-Savart Laws as:

$$v_L(x) = \frac{1}{4\pi} \int_0^1 \frac{\varepsilon}{|x - \eta| [(\varepsilon + \kappa)^2 (x + \eta)^2 + 1]}^{1.5} \bar{\Gamma}(\eta) d\eta$$

$$v_T(x) = \frac{-1}{4\pi} \sum_{n=1}^b \frac{d\bar{\Gamma}}{d\eta}$$

$$\int_0^\infty \frac{\eta^2 (1 + \varepsilon^2 \eta^2) - x(1 + \varepsilon^2 x^2)^{0.5} \eta (1 + \varepsilon^2 \eta^2)^{0.5} \cos(\bar{\psi} + \delta - \zeta)}{|\bar{R}|^3} d\psi d\eta$$

where

$$|\bar{R}|^2 = \eta^2 (1 + \varepsilon^2 \eta^2) + x^2 (1 + \varepsilon^2 x^2)$$

$$- 2x(1 + \varepsilon^2 x^2)^{0.5} \eta (1 + \varepsilon^2 \eta^2)^{0.5} \cos(\bar{\psi} + \delta - \zeta) + (v_c \psi - \kappa \eta^2 + \kappa x^2)^2$$

and

$$\bar{\psi} = \psi + 2\pi \frac{(n-1)}{b}; \quad \zeta = \tan^{-1}(\varepsilon x); \quad \delta = \tan^{-1}(\varepsilon \eta)$$

Note that v_L is the induced velocity due to the bound vortex of an inplane curved blade. We neglect the effect of the curved lifting-line from other blades. However, the influence of the trailing vortex lines from other blades has been included.

Equations for aerodynamic function:

Once $\bar{\Gamma}(x_j)$ and $v_i(x_j)$ are obtained along the spanwise position x_j , (by solution of governing equation) the total lift coefficient C_L , total induced drag coefficient C_{D_i} , and total induced power coefficient C_{P_i} are:

$$\frac{C_L}{\theta_o} = \frac{\int_0^R \rho r \Omega \Gamma(r) dr}{\rho (R\Omega)^2 S_R \theta_o} = AR \sum_j x_j \bar{\Gamma}(x_j) \Delta x_j$$

$$\frac{C_{D_i}}{\theta_o} = \frac{\int_0^R \rho r \Omega w_i(r) \Gamma(r) dr}{\rho (R\Omega)^2 S_R \theta_o} = AR \sum_j x_j \bar{\Gamma}(x_j) v_i(x_j) \Delta x_j$$

$$\frac{C_{P_i}}{\theta_o} = v_c \frac{C_L}{\theta_o} + \frac{C_{D_i}}{\theta_o}$$

$$= v_c AR \sum_j x_j \bar{\Gamma}(x_j) \Delta x_j + AR \sum_j x_j \bar{\Gamma}(x_j) v_i(x_j) \Delta x_j$$

where S_R is the blade area and is equal to Rc_c . (Note that our definition of S_R is different from those normally used in the helicopter field.) If we divide the equation of total induced power coefficient C_{P_i} by C_{D_i} , it gives an index to judge how good a rotor is by the use of lift-drag ratio, C_L/C_{D_i} . This design index is slightly different from those in the fixed-wing field²⁻⁵, which use C_L^2/C_{D_i} .

Governing equations for derivatives of circulation:

To obtain aerodynamic derivatives, we use the concept developed by Yates in Ref. 16. Take partial derivative of Eq. (1) with respect to a typical design variable denoted Q as:

$$\frac{\partial}{\partial Q} \left\{ \frac{\sigma a}{2K} c(x) [x \bar{\theta}(x) - v(x)] \right\} = \frac{\partial}{\partial Q} \left\{ \frac{b}{\pi} \bar{\Gamma}(x) \right\} \quad (2)$$

Solve Eq. (2) for the derivative of circulation, $\partial \bar{\Gamma} / \partial Q$. The governing equations for the derivative of circulation with respect to each shape design variable can be expressed as:

$$\frac{K AR}{\pi c} \frac{\partial \bar{\Gamma}}{\partial \lambda} + \frac{\partial v}{\partial \lambda} = \left\{ \frac{K AR y}{\pi c [1+y(1+\lambda)]} - \frac{\partial}{\partial \lambda} \left(\frac{K AR}{\pi c} \right) \right\} \bar{\Gamma} \quad (3)$$

$$\frac{K AR}{\pi c} \frac{\partial \bar{\Gamma}}{\partial \beta} + \frac{\partial v}{\partial \beta} = \left\{ \frac{0.5 K AR y^{1/2} \ln y}{\pi c \beta^2} - \frac{\partial}{\partial \beta} \left(\frac{K AR}{\pi c} \right) \right\} \bar{\Gamma} \quad (4)$$

$$\frac{K AR}{\pi c} \frac{\partial \bar{\Gamma}}{\partial p} + \frac{\partial v}{\partial p} = \left\{ \frac{K AR \ln(1-y^{1/2})}{\pi c \beta^2} - \frac{\partial}{\partial p} \left(\frac{K AR}{\pi c} \right) \right\} \bar{\Gamma} \quad (5)$$

$$\frac{K AR}{\pi c} \frac{\partial \bar{\Gamma}}{\partial AR} + \frac{\partial v}{\partial AR} = \frac{-K \bar{\Gamma}}{\pi c} \quad (6)$$

$$\frac{K AR}{\pi c} \frac{\partial \bar{\Gamma}}{\partial \tau} + \frac{\partial v}{\partial \tau} = x \frac{\partial \bar{\theta}}{\partial \tau} \quad (7)$$

$$\frac{K AR}{\pi c} \frac{\partial \bar{\Gamma}}{\partial \delta} + \frac{\partial v}{\partial \delta} = x \frac{\partial \bar{\theta}}{\partial \delta} \quad (8)$$

$$\frac{K AR}{\pi c} \frac{\partial \bar{\Gamma}}{\partial \kappa} + \frac{\partial v}{\partial \kappa} = 0 \quad (9)$$

$$\frac{K AR}{\pi c} \frac{\partial \bar{\Gamma}}{\partial \epsilon} + \frac{\partial v}{\partial \epsilon} = 0 \quad (10)$$

where $\partial v / \partial Q$, in Eqs. (3)-(8), is expressed as:

$$\frac{\partial v(x)}{\partial Q} = \frac{-1}{4\pi} \sum_{n=1}^b \int_0^1 \frac{d(\partial \bar{\Gamma} / \partial Q)}{d\eta} \int_0^\infty \frac{\eta^2 (1+\epsilon^2 \eta^2) - x\eta \sqrt{(1+\epsilon^2 x^2)(1+\epsilon^2 \eta^2)} \cos(\bar{\psi} + \delta - \zeta)}{|\bar{R}|^3} d\psi d\eta \quad (11)$$

However, $\partial v / \partial \kappa$ and $\partial v / \partial \epsilon$ have the following forms:

$$\frac{\partial v(x)}{\partial \kappa} = \frac{-1}{4\pi} \sum_{n=1}^b \int_0^1 \frac{d(\partial \bar{\Gamma} / \partial \kappa)}{d\eta} \int_0^\infty \frac{\eta^2 (1+\epsilon^2 \eta^2) - x\eta \sqrt{(1+\epsilon^2 x^2)(1+\epsilon^2 \eta^2)} \cos(\bar{\psi} + \delta - \zeta)}{|\bar{R}|^3} d\psi d\eta$$

$$+ \frac{3}{4\pi} \int_0^1 \sum_{n=1}^b \frac{d\bar{\Gamma}}{d\eta} \int_0^\infty \frac{(\eta^2 - x\eta \cos(\bar{\psi} + \delta - \zeta))(\eta^2 - x^2)(v_c \psi - \kappa \eta^2 + \kappa x^2)}{|\bar{R}|^5} d\psi d\eta \quad (12)$$

$$\frac{\partial v(x)}{\partial \epsilon} = \frac{-1}{4\pi} \sum_{n=1}^b \int_0^1 \frac{d(\partial \bar{\Gamma} / \partial \epsilon)}{d\eta} \int_0^\infty \frac{\eta^2 (1+\epsilon^2 \eta^2) - x\eta \sqrt{(1+\epsilon^2 x^2)(1+\epsilon^2 \eta^2)} \cos(\bar{\psi} + \delta - \zeta)}{|\bar{R}|^3} d\psi d\eta$$

$$- \frac{1}{4\pi} \sum_{n=1}^b \int_0^1 \frac{d\bar{\Gamma}}{d\eta} \int_0^\infty \frac{1}{|\bar{R}|^3} [2\epsilon \eta^4 - \epsilon x \eta (x^2 + \eta^2 + 2\epsilon^2 x^2 \eta^2) \cos(\bar{\psi} + \delta - \zeta) + x\eta (\epsilon^2 x \eta - 1)(x - \eta) \sin(\bar{\psi} + \delta - \zeta)] d\psi d\eta$$

$$+ \frac{3}{4\pi} \int_0^1 \sum_{n=1}^b \frac{d\bar{\Gamma}}{d\eta} \int_0^\infty \frac{\eta^2 (1+\epsilon^2 \eta^2) - x\eta \sqrt{(1+\epsilon^2 x^2)(1+\epsilon^2 \eta^2)} + \cos(\bar{\psi} + \delta - \zeta)}{|\bar{R}|^5} [\epsilon \eta^4 + \epsilon x^4 - \epsilon x \eta (x^2 + \eta^2 + 2\epsilon^2 x^2 \eta^2) \cos(\bar{\psi} + \delta - \zeta) + x\eta (\epsilon^2 x \eta - 1)(x - \eta) \sin(\bar{\psi} + \delta - \zeta)] d\psi d\eta$$

$$+ \frac{1}{4\pi} \int_0^1 \frac{1+(x+\eta)^2(\varepsilon+\eta-3)(\varepsilon+\eta)}{|x-\eta|[(\varepsilon+\kappa)^2(x+\eta)^2+1]^{2.5}} \bar{\Gamma}(\eta) d\eta \quad (13)$$

Once $\partial \bar{\Gamma}(x_i)/\partial Q$ and $\partial v_T(x_i)/\partial Q$ are obtained along the spanwise position x_i , (by solution of governing equation) and the $\partial C_L/\partial Q$, $\partial C_{D_i}/\partial Q$, and $\partial C_{P_i}/\partial Q$ can be easily found through the chain rules from equations of C_L , C_{D_i} , and C_{P_i} .

Numerical Solutions

Solutions for circulation:

Two numerical methods have been developed to solve Eq. (1) for circulation. These are (a) the Multhopp Interpolation technique, which is a special case of Fourier Series method and widely used in fixed-wing cases and (b) the Vortex Lattice Method, which can be easily extended for lifting-surface theory.

Multhopp Interpolation Technique: The idea is to transform the spanwise coordinate by :

$$x = \frac{1 - \cos(\varphi)}{2}$$

and replaces the downwash integral $v_T(x)$ in Eq. (1) with midpoint trapezoidal rule summation to obtain:

$$v_T(x_i) = \frac{-1}{4\pi} \int_0^b \sum_{n=1}^M \frac{d\bar{\Gamma}}{d\eta} \frac{\eta^2(1+\varepsilon^2\eta^2) - x\eta\sqrt{(1+\varepsilon^2x^2)(1+\varepsilon^2\eta^2)} \cos(\bar{\psi} + \delta - \zeta_i)}{|\vec{R}_i|^3} d\psi d\eta \quad (14)$$

$$\approx \frac{-1}{4M} \sum_{l=1}^M \left(\frac{d\bar{\Gamma}}{d\varphi} \right)_l P_{il}$$

where

$$P_{il} = \sum_{n=1}^M \int_0^b \frac{\eta_l^2(1+\varepsilon^2\eta_l^2) - x_i\eta_l\sqrt{(1+\varepsilon^2x_i^2)(1+\varepsilon^2\eta_l^2)} \cos(\bar{\psi} + \delta - \zeta_i)}{|\vec{R}_{ij}^*|^3} d\psi \quad (14-a)$$

$$|\vec{R}_i|^2 = \eta^2(1+\varepsilon^2\eta^2) + x_i^2(1+\varepsilon^2x_i^2) - 2x_i\eta\sqrt{(1+\varepsilon^2x_i^2)(1+\varepsilon^2\eta^2)} \cos(\bar{\psi} + \delta - \zeta_i) + (v_c\psi - \kappa\eta^2 + \kappa x_i^2)^2$$

and

$$|\vec{R}_{ij}^*|^2 = \eta_l^2(1+\varepsilon^2\eta_l^2) + x_i^2(1+\varepsilon^2x_i^2) - 2x_i\eta_l\sqrt{(1+\varepsilon^2x_i^2)(1+\varepsilon^2\eta_l^2)} \cos(\bar{\psi} + \delta - \zeta_i) + (v_c\psi - \kappa\eta_l^2 + \kappa x_i^2)^2$$

Equation (14) represents the downwash due to M trailing vortices of strength $(d\bar{\Gamma}/d\varphi)_l (\pi/M)$, which are along the helical wake and are located at:

$$\varphi_l = \frac{(l-0.5)\pi}{M}, \quad l = 1, \dots, M$$

with control points located at:

$$\varphi_i = \frac{i\pi}{M}, \quad i = 1, \dots, M-1$$

The Multhopp Interpolation formula suggests that:

$$\bar{\Gamma}(\varphi) = \frac{2}{M} \sum_{j=1}^{M-1} \bar{\Gamma}_j \sum_{m=1}^{M-1} \sin(m\varphi_j) \sin(m\varphi) \quad (15)$$

where $\bar{\Gamma}_j$ represents $\bar{\Gamma}(\varphi_j)$ and

$$\varphi_j = \frac{j\pi}{M}, \quad j = 1, \dots, M-1$$

Equation (15) is based on the following orthogonality property:

$$\frac{2}{M} \sum_{m=1}^{M-1} \sin(m\varphi_j) \sin(m\varphi_i) = \delta_{ij}$$

here, δ_{ij} is the *Kronecker-delta*. When Eq. (15) is used in Eq. (14), $v_T(x_i)$ reduces to :

$$v_T(x_i) = \frac{-1}{2M^2} \sum_{l=1}^M \sum_{j=1}^{M-1} \bar{\Gamma}_j \sum_{m=1}^{M-1} m \sin(m\varphi_j) \cos(m\varphi_i) P_{il} \quad (16)$$

$$= \sum_{j=1}^{M-1} A_{ij}^T \bar{\Gamma}_j$$

where

$$A_{ij}^T = \frac{-1}{2M^2} \sum_{l=1}^M \sum_{m=1}^{M-1} m \sin(m\varphi_j) \cos(m\varphi_i) P_{il}$$

here, A_{ij}^T are the influence coefficients of trailing vortices and can be solved for by numerical methods without any difficulty, if x_i and η_l are specified and P_{il} can be calculated. However, P_{il} contains an integral with an infinite upper limit and no closed-form solution exists. A numerical solution has been developed by the current authors in Ref. 17 to calculate P_{il} semi-analytically. Results are very accurate with minimal computation time.

Similarly, if we replace the downwash integral $v_L(x)$ in Eq. (1) with the Multhopp Interpolation formula at control points x_i , then $v_L(x_i)$ becomes:

$$v_L(x_i) = \frac{1}{4\pi} \int_0^1 \frac{\varepsilon}{|x_i - \eta| [(\varepsilon + \kappa)^2(x_i + \eta)^2 + 1]^{1.5}} \bar{\Gamma}(\eta) d\eta$$

$$\approx \frac{\varepsilon}{4\pi} \int_0^1 \frac{1}{|x_i - \eta|} \bar{\Gamma}(\eta) d\eta$$

$$= \frac{\varepsilon}{2M\pi} \sum_{j=1}^{M-1} \bar{\Gamma}_j \sum_{m=1}^{M-1} \sin(m\varphi_j) \int_0^\pi \frac{\sin(m\varphi) \sin(\varphi) d\varphi}{|\cos(\varphi_j) - \cos(\varphi)|}$$

$$= \sum_{j=1}^{M-1} A_{ij}^L \bar{\Gamma}_j \quad (17)$$

where

$$A_{ij}^L = \frac{\varepsilon}{2M\pi} \sum_{m=1}^{M-1} \sin(m\varphi_j) \int_0^\pi \frac{\sin(m\varphi) \sin(\varphi) d\varphi}{|\cos(\varphi_j) - \cos(\varphi)|}$$

here, A_{ij}^L are the influence coefficients of bound vortices and contains an integral with a Log singularity. This integral diverges when φ_i is equal to φ . It should be interpreted in other than the usual sense. The answer is given by the concept of the "finite part" established by Hadamard¹⁰ and has been applied to fixed-wing cases in Ref. 11. In Appendix A of this paper, we show that A_{ij}^L can be obtained analytically if $\bar{\Gamma}$ is expressed as the Fourier sine series. In Eq. (17), we apply the assumption of small $(\kappa + \varepsilon)^2$. Cases for large $(\kappa + \varepsilon)^2$ can also be calculated elegantly and are described in Appendix A.

Finally, substitution of Eqs. (16) and (17) for the downwash in Eq. (1) and application of resulting equation at spanwise location φ_i gives a $(M-1) \times (M-1)$ matrix equation for $M-1$ values of $\bar{\Gamma}$'s as:

$$\sum_{j=1}^{M-1} A_{ij} \bar{\Gamma}_j = x_i \bar{\theta}_i - v_c / \theta_o, \quad i = 1, \dots, M-1 \quad (18)$$

where

$$A_{ij} = A_{ij}^L + A_{ij}^T + \delta_{ij} K AR / (\pi \bar{c}_i)$$

Once $\bar{\Gamma}_j$'s are obtained, C_L , C_{D_i} , C_L / C_{D_i} , and C_P , can be calculated as described before. The local induced velocity $v_i(x_i)$ is found as:

$$v_i(x_i) = v_T(x_i) + v_L(x_i) = \sum_{j=1}^{M-1} (A_{ij}^L + A_{ij}^T) \bar{\Gamma}_j$$

Vortex Lattice Method (VLM): The conventional VLM discretizes the rotor span into a number of panels, M . The trailing point is located at the boundary of each panel, and the control point is placed at the midpoint of each panel. However, there is a controversy as how to choose collocation points. Several papers^{7,15,18,19} have shown that this conventional VLM converges slowly and does not appear to approach the correct limit for fixed-wing cases. A similar phenomenon has been found for rotary-wing cases in Ref. 15. All these papers suggest that the semi-circle collocation points, which are defined in the Multhopp Interpolation technique, are essentially required for VLM when the fastest rate of convergence is desired. Most researchers have selected collocation points arbitrarily or equally-spacedly. Such selection may be adequate for aerodynamic analysis. But, it is not suitable for aerodynamic sensitivity analysis.

The VLM in this paper uses the semi-circle collocation points to solve Eq. (1). For the trailing downwash integral $v_T(x)$ in Eq. (1), we apply the first order finite

difference on $\bar{\Gamma}$ with midpoint trapezoidal rule summation to obtain A_{ij}^T as:

$$A_{ij}^T = \frac{1}{4\pi} (P_{ij} - P_{ij+1}) \quad (19)$$

where P_{ij} is defined by the Eq. (14-a). A common way to calculate A_{ij}^L is described in Ref. 6. The straight vortex filament with unit circulation is stretched from each trailing point. Then, the sum of this vortex filament and Eq. (19) is equivalent to the influence of a horseshoe vortex at panel j at control point x_i . However, this approach is not completely rigorous, since the curved lifting-line has been approximated by several straight vortex filaments. Another way (used in this paper) to solve the problem is to apply Eqs. (17) and (19) for downwash calculation in Eq. (18), since both equations have the same control points.

Solutions for derivatives of circulation:

Two numerical approaches can be used to solve Eq. (2) for derivatives of circulation and result in same numerical solutions. The first one is to discretize Eq. (2) by following the path of discretizations used for solutions of circulation. The second approach simply differentiates a set of equations (expressed in equation number (18)) with respect to a particular design variable Q . Then, we solve a matrix equation for $M-1$ values of derivatives of circulation, which can be expressed as:

$$\sum_{j=1}^{M-1} A_{ij} \frac{\partial \bar{\Gamma}_j}{\partial Q} = \frac{\partial (x_i \bar{\theta}_i)}{\partial Q} - \sum_{j=1}^{M-1} \frac{\partial A_{ij}}{\partial Q} \bar{\Gamma}_j, \quad i = 1, \dots, M-1 \quad (20)$$

where

$$\frac{\partial A_{ij}}{\partial Q} = \frac{\partial A_{ij}^L}{\partial Q} + \frac{\partial A_{ij}^T}{\partial Q} + \delta_{ij} \frac{\partial [K AR / (\pi \bar{c}_i)]}{\partial Q}$$

Equation (20) is a set of linear equations and can be solved if the right hand side of Eq. (20) is known. However, not all terms exist for all cases. For example, the term $\partial A_{ij}^L / \partial Q$ exists for nonzero inplane curvature ε ; the term $\partial (x_i \bar{\theta}_i) / \partial Q$ is valid for parameters of twist distribution; and the term $\partial [K AR / (\pi \bar{c}_i)] / \partial Q$ exists only for parameters of chord distribution. The procedures are systematically analogous to analyses for circulation which are described in the previous section.

Results

Test problems

Equations (1) and (2) have been normalized with respect to some reference quantities. The following parametric values will be used in this paper for the reference-blade: $\theta_o = 1$, $\lambda = 1$, $p = \beta = 0.5$, $v_c = 0.06$, $\delta = 0.6$, $\kappa = \varepsilon = \tau = m = 0$, $AR = 10$ (or $\sigma = 0.0637$);

$b = 2$. In some cases, we compare results with different chord distributions which are defined as:

- (1) elliptic blades: $\lambda = 1, p = 0.5, \beta = 0.5$
- (2) rectangular blades: $\lambda = 1, p = 0, \beta = 0$
- (3) triangular blades: $\lambda = 0, p = 0, \beta = 0$
- (4) tapered blades: $\lambda = 1/3, p = 0, \beta = 0$
- (5) parabolic blades: $\lambda = 1, p = 0.5, \beta = 0.5$

where all blades have the same solidity based on the same blade area (i.e., $m = 0$). Figure 6 shows the normalized quarter chord distribution along the spanwise direction for these blades.

Effect of number of panels or terms, M

Table 1 is the convergence results of circulation ($\bar{\Gamma}$) and derivative ($\partial\bar{\Gamma}/\partial\kappa$) with respect to out-of-plane curvature (κ) for an elliptic blade at midspan $x = 0.5$. This table implies that aerodynamic functions and derivatives are equally accurate from both Multhopp Interpolation formula and VLM but are sensitive to the number of discretization panels and terms M . Also, the analytical methods are confirmed by the finite difference method which solves Eq. (1) twice with $\kappa = 0$ and $\kappa = 0.001$. The similar accuracy is also obtained for C_L, C_{D_i}, C_{P_i} and its derivatives. For a reasonable number of terms or panels ($M=20$), the methods provide approximately 4 digits of accuracy for aerodynamic functions and 2 digits of accuracy for aerodynamic derivatives. The following results for this paper are based on $M=20$ by the Multhopp Interpolation formula.

Effect of curvatures of the the lifting line

Figures 7-9 are results of C_L, C_{D_i} and C_L/C_{D_i} as functions as out-of-plane curvature κ for various blade shapes. Figure 7 shows that C_L is nearly proportional to κ . However, C_{D_i} is nearly constant for each blade shape shown in Fig. 8. Results of C_L/C_{D_i} in Fig. 9 have the similar trend as those for C_L . Therefore, by curving the blades in the opposite direction of thrust (i. e., $\kappa > 0$), the rotor would be more efficient. The reason is because the trailing vortex lines move away from the blades when κ is increased. Consequently, the induced velocity along the span is decreased and the thrust is increased. This phenomenon is clearly shown in Figs. 10 and 11. Figure 10 presents the variation of circulation along the span. Figure 11 presents the variation of induced velocity. It is interesting to note that the inboard region ($x = 0 \rightarrow 0.8$) is improved when κ is increased. Unfortunately, such a blade is physically unrealizable due to the fact that the helicopter blades have to cone up (i. e., $\kappa < 0$) to compensate the centrifugal forces for structural considerations.

For effects of inplane curvature ϵ , similar trends of results have been found as shown in Fig. 12 for C_L/C_{D_i} .

The rotor lift-drag ratio will improve when ϵ is increased. Therefore, by sweeping the blades backward (i. e., $\epsilon > 0$), the rotor would be more efficient. Figure 13 presents the variation of circulation along the span. Figure 14 presents the variation of induced velocity. Note from Figs. 13 and 14 that the outboard region ($x = 0.4 \rightarrow 1.0$) has been improved when ϵ is increased.

One might wonder how much additional improvement might be made by the combinations of κ and ϵ . One answer is shown in Fig. 15 where contour lines of C_L/C_{D_i} are plotted for different values of κ and ϵ . It clearly shows that positive κ and ϵ can always improve the lift-drag ratio, C_L/C_{D_i} , of a straight blade (i.e., $\kappa = \epsilon = 0$). For example, numerical results indicate that making $\kappa = \epsilon = 0.3$ can increase C_L/C_{D_i} by 16 percent as compared to the straight blade. However, making $\kappa = \epsilon = -0.3$ can decrease this ratio by 10.4 percent. Also, Fig. 15 indicates that the effect of κ is slightly stronger than the effect of ϵ . Figure 16 presents the contour lines of $\partial(C_L/C_{D_i})/\partial\epsilon$ which represent the slope of Fig. 15 with respect to ϵ . The peak value occurs around $\epsilon = 0$ and $\kappa = 0.05$. It is observed, from Figs. 10 and 13, that dual peak circulations appear. This is very common for rotors which do not have an ideal twist. Unlike the conventional blade element theory, the three dimensional undistorted wake model in this paper can catch this "dual peak" phenomenon. Cases for different twist distributions and inflow ratios have also been investigated. All results indicate that positive κ and ϵ are very promising parameters to increase lift in the inboard and outboard regions respectively without introducing an additional induced drag.

Effect of chord distribution

Figures 7,8,9, and 12 indicate that elliptic and parabolic blades are better than rectangular blades. For example, parabolic blades always provide more lift with the same induced drag than rectangular blades. Elliptic blades can provide the maximum C_L and C_{D_i} . For all blade shapes, a case with larger C_L is always accompanied with larger C_{D_i} and vice versa. Although triangular blades provide the maximum C_L/C_{D_i} , they are not desirable. The reason is because C_L and C_{D_i} are also very small and this design is unrealistic due to the need for larger C_L to provide sufficient lift. A compromise design is by the use of tapered blades, as shown in Figs. 7 and 9.

Such blades can provide the minimum desired lift with reasonable lift-drag ratio.

The results for effect of aspect ratio are shown in Fig. 17-20. Figure 17 indicates that C_L grows with increased aspect ratios for all blades. However, C_{D_i} , shown in Fig.

18, increases when aspect ratio is smaller than 9. Then, it decreases with a larger aspect ratio where the flow field is approaching the two-dimensional case and the induced velocity tends to decrease along the span. Figure 19 shows the results of C_L/C_{D_i} and indicates that C_L/C_{D_i} is

nearly proportional to aspect ratio. Figure 20 is the result for the derivative of C_L/C_{D_i} . Increasing the aspect ratio is increasing the lift-drag ratio. However, the resulting increase in blade weight would tend to limit the increase in aspect ratio. Results for variations of p , β , and λ and its derivatives have also obtained and will be presented for C_L/C_{D_i} only. Figure 21 indicates that variation of C_L/C_{D_i} ,

with tip length parameter, β , for an elliptic blade has the minimum value around $\beta \approx 0.25$. This minimum value is around $p \approx 0.20$ with tip shape parameter, p , as shown in Fig. 22. Figure 23 shows that variation of C_L/C_{D_i} with taper ratio, λ , for an elliptic blade has the maximum value at $\lambda = 0.0$ which represents the triangular shape.

Effect of twist distribution

The results for effect of τ are shown in Figs. 24-26. Figure 24 indicates that C_L is nearly proportional to τ . This is due to the fact that a large value of τ provides large angles of twist along the span. It is interesting to note that, from Fig. 25, C_{D_i} decreases when τ is negative.

Consequently, An optimum design of a rotor can be specified around $-0.05 < \tau < 0.05$, which are shown in Fig. 26 with maximum values of C_L/C_{D_i} . The results for the effect of δ are shown in Fig. 27 which presents the variation of C_L/C_{D_i} . It seems to imply that an optimum

design is around $0.35 < \delta < 0.40$. However, This is only partially true due to the fact that a small value of τ always provides small values of C_L and C_{D_i} .

Conclusions

In summary, this paper offers analytical capability for aerodynamic parametric studies and sensitivity analysis of rotary wings in axial flight by using a 3-dimensional undistorted wake model in curved lifting-line theory.

Analytical expressions are developed for aerodynamic functions and sensitivity derivatives with respect to shape design variables including taper ratio, tip length, tip shape, aspect ratio, inplane curvature, out-of-plane curva-

ture, twist ratio, and twist shape. The governing equations of aerodynamic functions and derivatives are solved by using both Multhopp Interpolation Technique and Vortex Lattice Method. Numerical results show that aerodynamic functions and derivatives are insensitive to discretization methods but are sensitive to the number of discretization panels. For example, for a reasonable number of terms or panels ($M=20$), the methods provide 4 digits of accuracy for aerodynamic functions and 2 digits of accuracy for aerodynamic derivatives.

Also, it is found that a rotor blade with out-of-plane and inplane curvature can theoretically increase lift in the inboard and outboard regions respectively without introducing an additional induced drag. However, positive out-of-plane curvature is physically undesirable due to structural considerations, while positive inplane curvature ϵ is easier to obtain.

Appendix A

In Eq. (17), the finite part (FP) for the following integral which contains a $1/|x|$ type singularity is defined in Ref. 11, Appen. A, as follows:

$$I = FP \int_0^1 \frac{f(\eta)}{|x_i - \eta|} d\eta = \lim_{\epsilon \rightarrow 0} \left[\int_0^{\eta-\epsilon} \frac{f(\eta)}{|x_i - \eta|} d\eta + \int_{\eta+\epsilon}^1 \frac{f(\eta)}{|x_i - \eta|} d\eta + 2f(x_i) \ln \epsilon \right] \quad (A-1)$$

If the variable in Eq. (A-1) is transformed from η to ϕ according to the semi-circle points, An equivalent equation can be obtained as follows:

$$I = FP \int_0^\pi \frac{f(\phi) \sin(\phi) d\phi}{|\cos(\phi_i) - \cos(\phi)|} = \lim_{\epsilon_\phi \rightarrow 0} \left[\int_0^{\phi-\epsilon_\phi} \frac{f(\phi) \sin(\phi) d\phi}{|\cos(\phi_i) - \cos(\phi)|} + \int_{\phi+\epsilon_\phi}^\pi \frac{f(\phi) \sin(\phi) d\phi}{|\cos(\phi_i) - \cos(\phi)|} + 2f(\phi_i) \ln \epsilon \right] \quad (A-2)$$

where

$$\epsilon = \frac{\epsilon_\phi}{2} \sin \phi$$

Equation (A-2) can be solved analytically if $f(\eta)$ can be expressed as the Fourier sine series. For example, let $f(\eta)$ be equal to $\sin(m\phi)$. Then,

$$I = FP \int_0^\pi \frac{\sin(m\phi) \sin(\phi) d\phi}{|\cos(\phi_i) - \cos(\phi)|} = \frac{1}{2} [G(\phi_i, m-1) - G(\phi_i, m+1)] \quad (A-3)$$

where

$$G(\phi_i, m) = FP \int_0^\pi \frac{\cos(m\phi) d\phi}{|\cos(\phi_i) - \cos(\phi)|}$$

The integral G is obtained from the recurrence relation:

$$G(\varphi_i, m+1) - 2 \cos(\varphi_i) G(\varphi_i, m) + G(\varphi_i, m-1) = \frac{4 \sin(m\varphi_i)}{m}$$

where the initial integrals are:

$$G(\varphi_i, 0) = \frac{4}{\sin(\varphi_i)} \ln(\sin(\varphi_i))$$

$$G(\varphi_i, 1) = 2\varphi_i - \pi + 4 \cot(\sin(\varphi_i)) \ln(\sin(\varphi_i))$$

Substituting Eq. (A-3) in Eq. (17) we obtain

$$A_{ij}^L = \frac{\varepsilon}{2M\pi} \sum_{m=1}^{M-1} \sin(m\varphi_j) \int_0^\pi \frac{\sin(m\varphi) \sin(\varphi) d\varphi}{|\cos(\varphi_i) - \cos(\varphi)|}$$

$$= \frac{\varepsilon}{4M\pi} \sum_{m=1}^{M-1} \sin(m\varphi_j) [G(\varphi_i, m-1) - G(\varphi_i, m+1)] \quad (A-4)$$

Equation (A-4) is only good for small $(\kappa + \varepsilon)^2$. For cases for large $(\kappa + \varepsilon)^2$, we use Multhopp interpolation formula for $h(\eta) \bar{\Gamma}(\eta)$ as:

$$h \bar{\Gamma} = \frac{2}{M} \sum_{j=1}^{M-1} (h \bar{\Gamma})_j \sum_{m=1}^{M-1} \sin(m\varphi_j) \sin(m\varphi)$$

where

$$h(\eta) = \frac{1}{[(\varepsilon + \kappa)^2 (x_i + \eta)^2 + 1]^{1.5}}$$

$$= \frac{1}{[(\varepsilon + \kappa)^2 (1 - 0.5 \cos(\varphi_i) - 0.5 \cos(\varphi_j))^2 + 1]^{1.5}} \quad (A-5)$$

Substituting Eq. (A-5) in Eq. (17) we obtain

$$A_{ij}^L = \frac{\varepsilon}{4M\pi [(\varepsilon + \kappa)^2 (1 - 0.5 \cos(\varphi_i) - 0.5 \cos(\varphi_j))^2 + 1]^{1.5}}$$

$$\sum_{m=1}^{M-1} \sin(m\varphi_j) [G(\varphi_i, m-1) - G(\varphi_i, m+1)]$$

Acknowledgements

This work was performed at the NASA Langley Research Center under NASA contract NAS1-19000 for Lockheed Engineering and Science Company, technical monitor Dr. Howard M. Adelman.

References

- ¹Sobieski, J., "The case for Aerodynamic Sensitivity Analysis," Sensitivity Analysis in Engineering, NASA CP-2457, 1986, pp. 77-96.
- ²Henderson, W. P., and Holmes B. J., "Induced Drag - Historical Perspective," SAE Aerotech '89 Conference, Anaheim, California, September 25-28, 1989.
- ³Burkett, C. W., "Reductions in Induced Drag by the use of Aft Swept Wing Tips," *Aeronautical Journal*, December 1989, pp. 400-405.

- ⁴Guermond J., "A Generalized Lifting-Line Theory for curved and Swept Wings," *L. Fluid Mech.*, 1990, vol. 211, pp. 497-513.

- ⁵Lowson, M., L., "Minimum Induced Drag for Wings with Spanwise Camber," *Journal of Aircraft*, Vol. 27, NO. 7, July, 1990, pp. 627-631.

- ⁶Rand, O. and Rosen A., "A Lifting Line Theory for Curved Helicopter Blades in Hovering and Axial Flight," *Journal of AHS*, vol. 29, no. 3, July 1984, pp. 3-10.

- ⁷Dejarnette, F. R., "Arrangement of Vortex Lattice on Subsonic Wings," Vortex-Lattice Utilization, NASA SP-405, 1976, pp. 301-323.

- ⁸Multhopp, H., "Methods for Calculating the Lift Distribution of Wings," British A.R.C., R&M 2884, January, 1950.

- ⁹Lamar, J. E., "A Modified Multhopp Approach for Predicting Lifting Pressures and Camber Shape for Composite Planforms in Subsonic Flow," NASA TN D-4427, July, 1968.

- ¹⁰Hadamard, J., *Lectures on Cauchy's Problem in Linear Differential Equation*, Dover, 1932, pp. 133-153.

- ¹¹Gibbs, C. P., *Lifting Surface Theory for Swept and Crank Subsonic Wings*, M. S. Thesis, North Carolina State University, Raleigh, 1985.

- ¹²Baskin, V. E., et al., *Theory of the Lifting Airscrew*, NASA TTF-823, 1976, pp. 147-163.

- ¹³Rand, O. and Rosen A., "The Aerodynamics of Helicopter Rotors in Hovering and Axial Flight Using Lifting-Line Models," TAE No. 485, TECHNION, Haifa, Israel, 1982.

- ¹⁴Ashenberg, J. and Weihs, D., "Curved Lifting-Line Theory for Thin Planar Wings," *Israel Journal of Technology*, Vol. 20, 1982, pp. 160-165.

- ¹⁵Chiu, Y. D., *Convergence of Discrete-Vortex Induced-Flow Calculations by Optimum Choice of Mesh*, Ph. D. Thesis, Georgia Institute of Technology, Atlanta, 1988.

- ¹⁶Yates, E. C., Jr., "Aerodynamic Sensitivity from Subsonic, Sonic, and Supersonic Unsteady, Nonplanar Lifting-Surface Theory," NASA TM 100502, 1987.

- ¹⁷Chiu, Y. D. and Peters, D. A., "Numerical Solutions of Induced Velocities by Semi-Infinite Tip Vortex Lines," *Journal of Aircraft*, Vol. 25, NO. 8, August, 1988, pp. 684-694.

- ¹⁸Lan, C., "A Quasi-Vortex-Lattice Method in Thin Wing Theory," *Journal of Aircraft*, Vol. 11, No. 9, 1974, pp. 518-527.

- ¹⁹Guermond J., "Collocation Methods and Lifting-Surfaces," *Eur. J. Mech., B/Fluids*, 8, No. 4, 1989, pp. 283-305.

Table 1 Convergence of circulation and derivatives with respect to κ for an elliptic blade at midspan.

Number of terms/ panels, M	circulation at midspan, $\bar{\Gamma}(0.5)$		circulation derivatives at midspan, $\partial \bar{\Gamma} / \partial \kappa$			
			Analytical Methods		Finite Difference Method	
	Multhopp	VLM	Multhopp	VLM	Multhopp	VLM
8	0.01950	0.01970	0.00468	0.00470	0.00468	0.00470
16	0.01951	0.01957	0.00468	0.00468	0.00467	0.00469
24	0.01951	0.01953	0.00470	0.00470	0.00470	0.00470
32	0.01951	0.01952	0.00471	0.00471	0.00471	0.00471
40	0.01951	0.01951	0.00472	0.00472	0.00472	0.00472
48	0.01951	0.01951	0.00473	0.00473	0.00473	0.00473
56	0.01951	0.01951	0.00474	0.00474	0.00474	0.00474

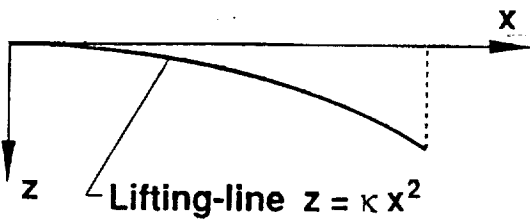


Fig. 1. Side view of rotor blade.

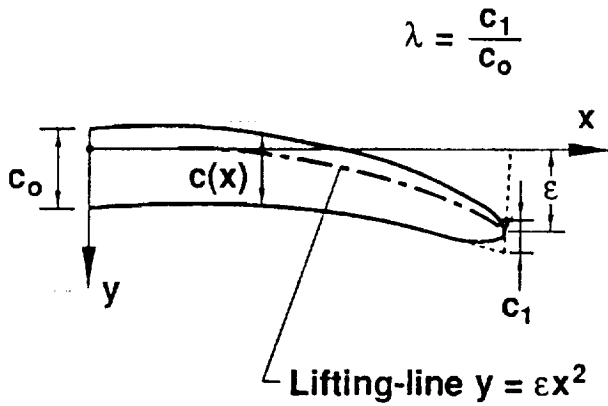


Fig. 2. Top view of rotor blade.

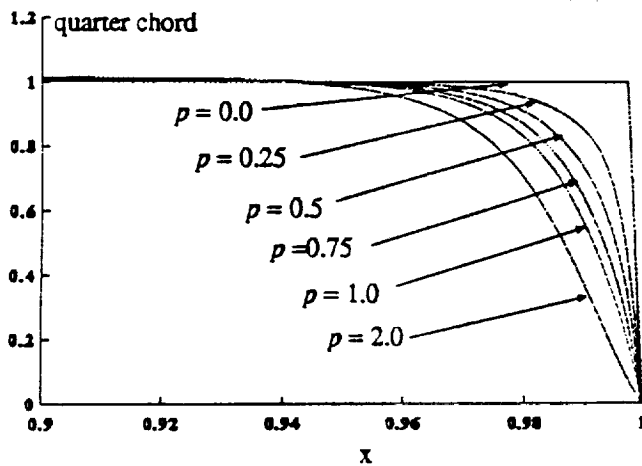


Fig. 3. Physical meaning of tip shape parameter, p , with $\beta = 0.01$; $\lambda = 1$.

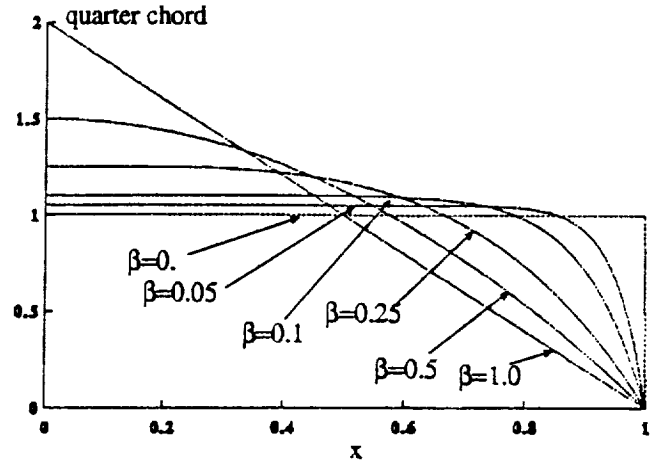


Fig. 4. Physical meaning of tip length parameter, β , with $p = 1$; $\lambda = 1$.

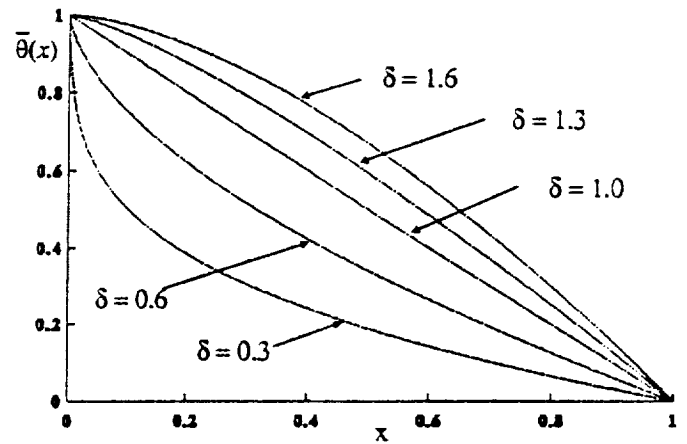


Fig. 5. Physical meaning of twist shape parameter, δ , with $\tau = 0$.

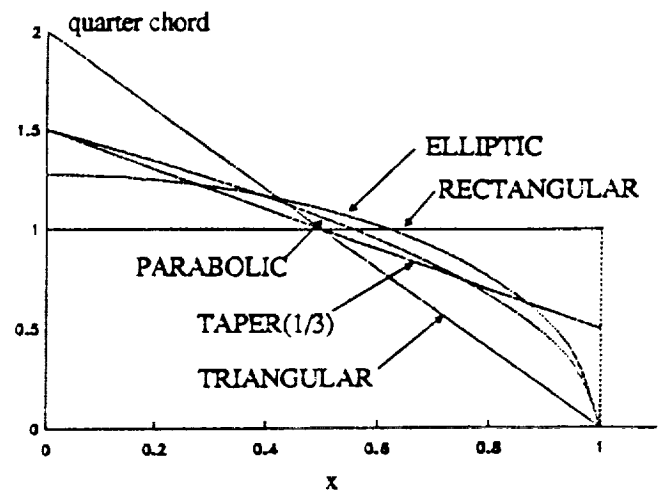


Fig. 6. Test cases for blades.

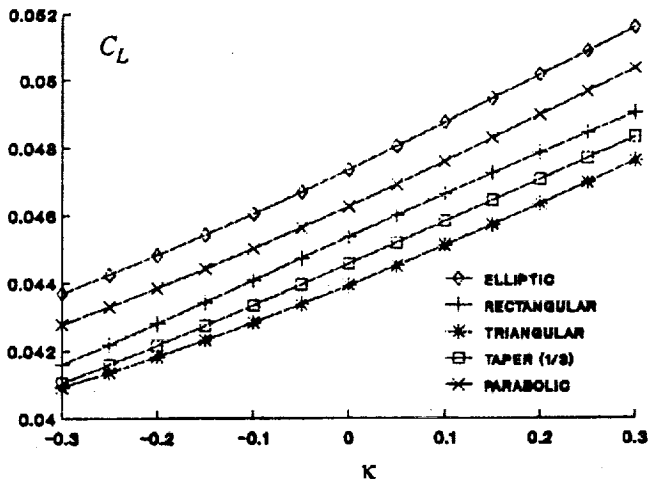


Fig. 7 Variation of C_L with out-of-plane curvature, κ , for various blade shapes.

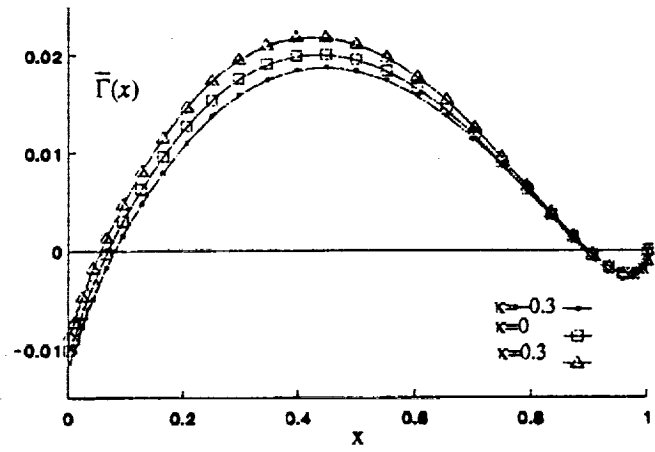


Fig. 10 Radial distributions of $\bar{\Gamma}(x)$ of elliptic blades for various κ .

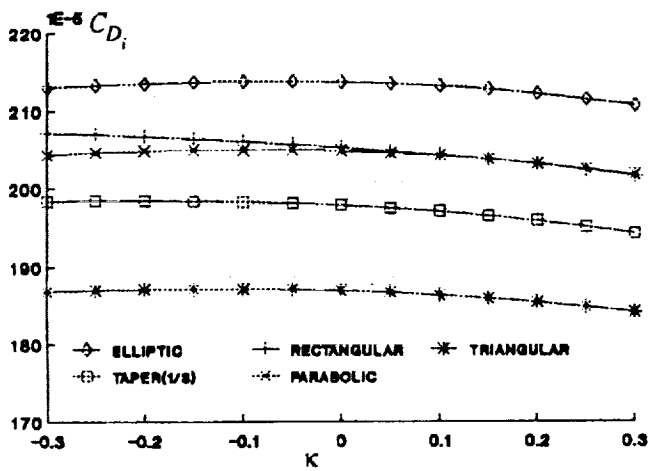


Fig. 8 Variation of C_{D_i} with out-of-plane curvature, κ , for various blade shapes.

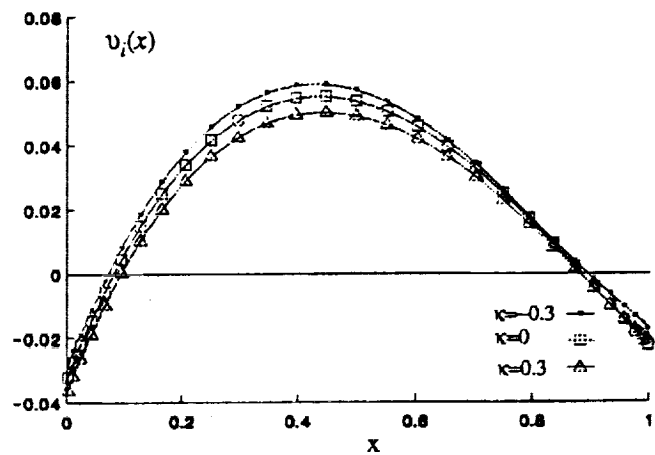


Fig. 11 Radial distributions of $v_i(x)$ of elliptic blades for various κ .

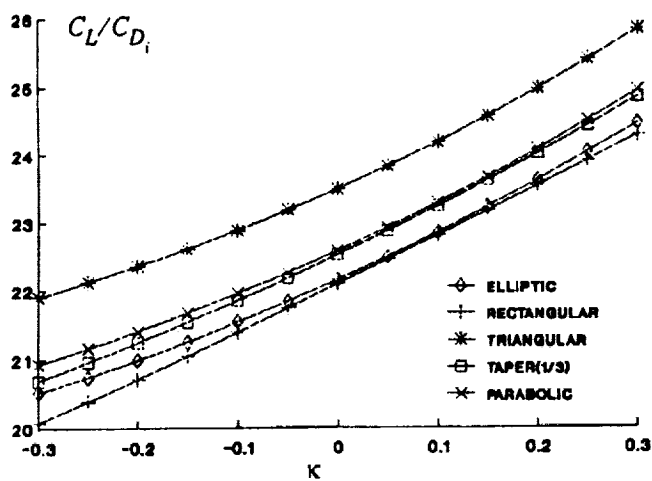


Fig. 9 Variation of C_L/C_{D_i} with out-of-plane curvature, κ , for various blade shapes.

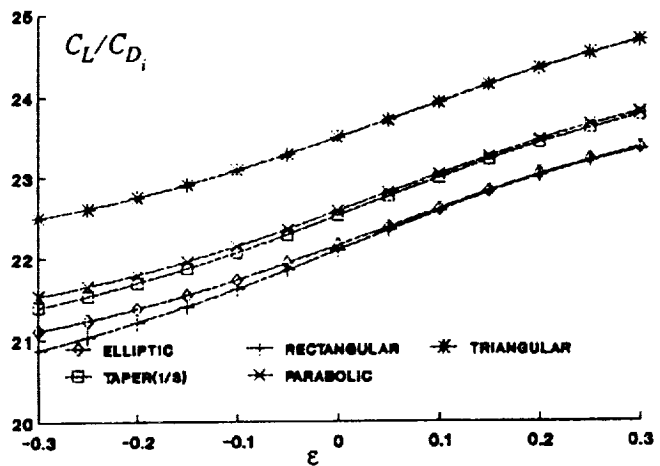


Fig. 12 Variation of C_L/C_{D_i} with inplane curvature, ϵ , for various blade shapes.

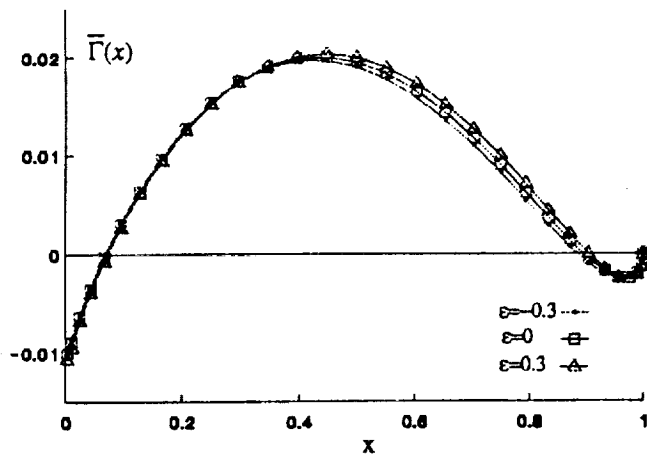


Fig. 13 Radial distributions of $\bar{\Gamma}(x)$ of elliptic blades for various ϵ .

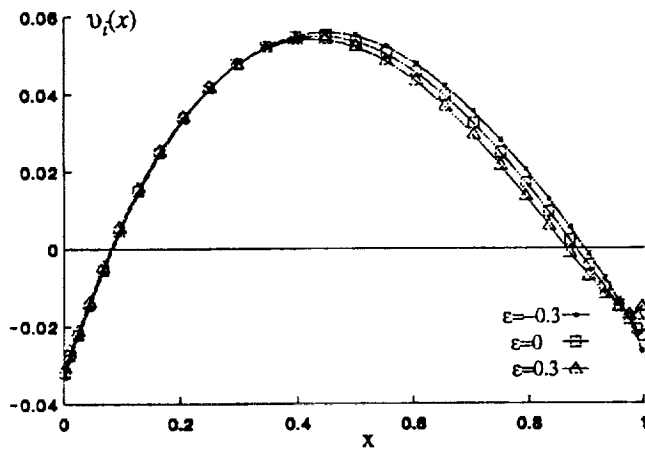


Fig. 14 Radial distributions of $v_i(x)$ of elliptic blades for various ϵ .

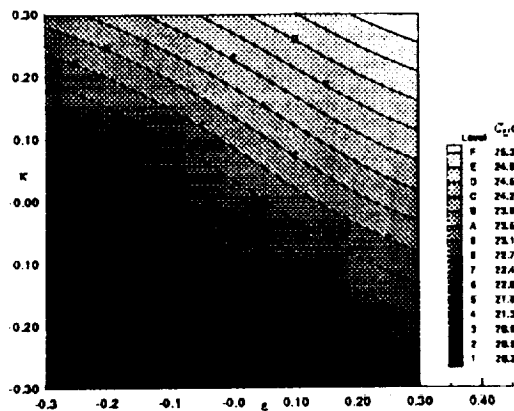


Fig. 15 Contour lines of C_L/C_{D_i} with κ and ϵ for an elliptic blade.

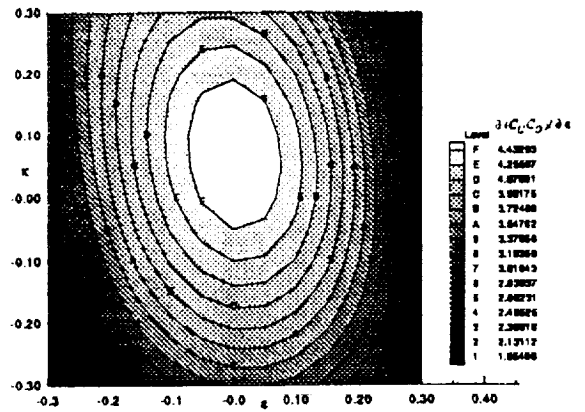


Fig. 16 Contour lines of derivatives of C_L/C_{D_i} with respect to ϵ with κ and ϵ for an elliptic blade.

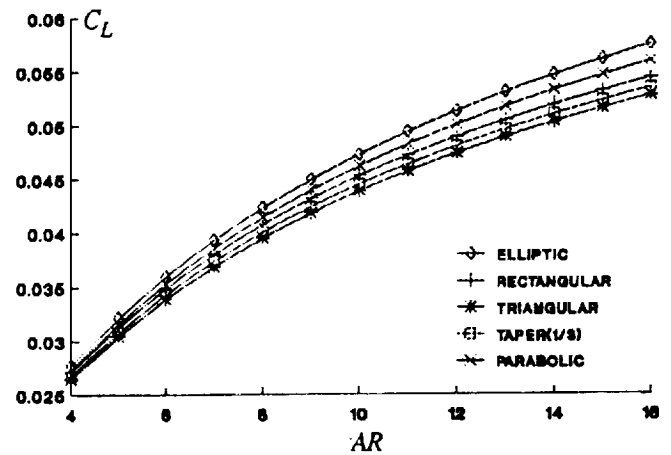


Fig. 17 Variation of C_L with aspect ratio, AR , for various blade shapes.

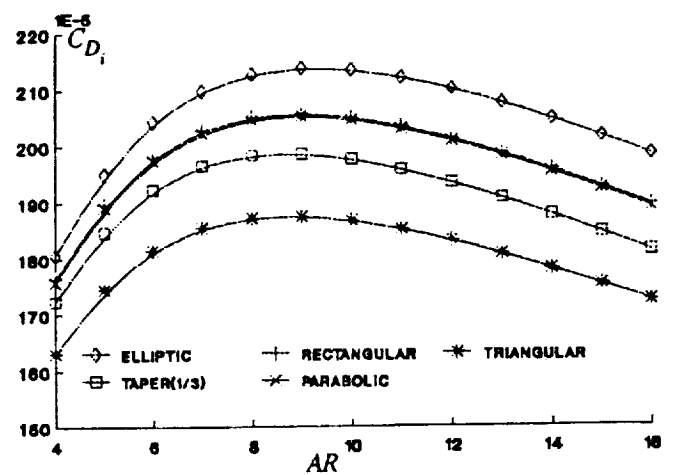


Fig. 18 Variation of C_{D_i} with aspect ratio, AR , for various blade shapes.

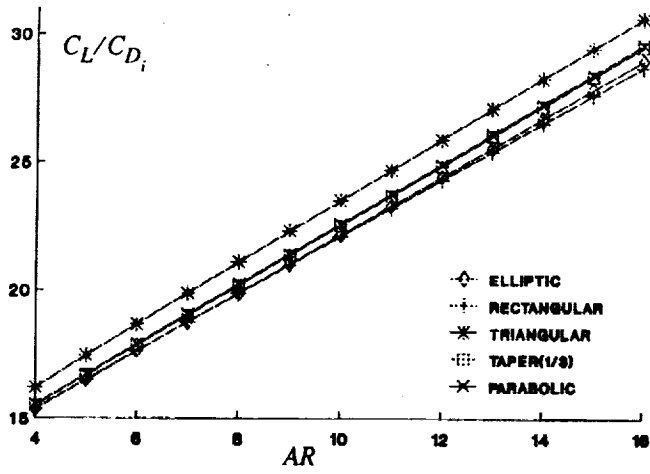


Fig. 19 Variation of C_L/C_{D_i} with aspect ratio, AR , for various blade shapes.

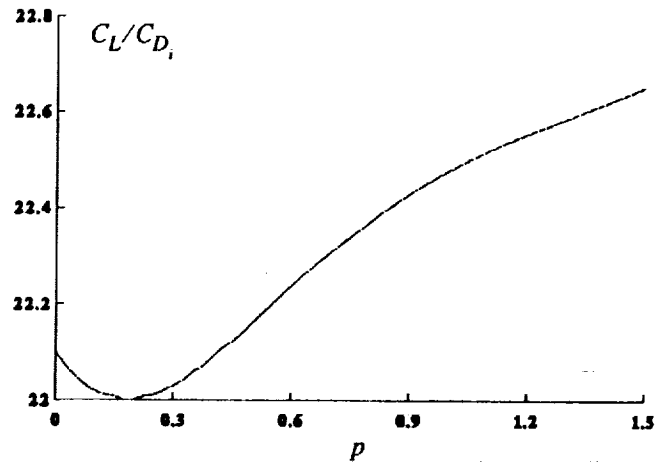


Fig. 22 Variation of C_L/C_{D_i} with tip shape parameter, p , for an elliptic blade.

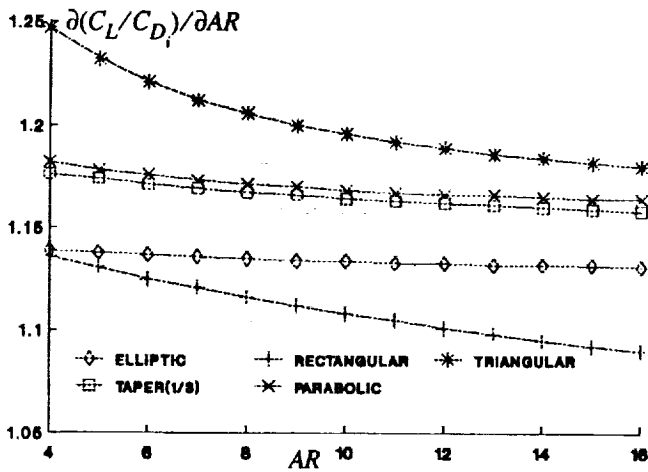


Fig. 20 Variation of derivative of C_L/C_{D_i} with aspect ratio, AR , for various blade shapes.

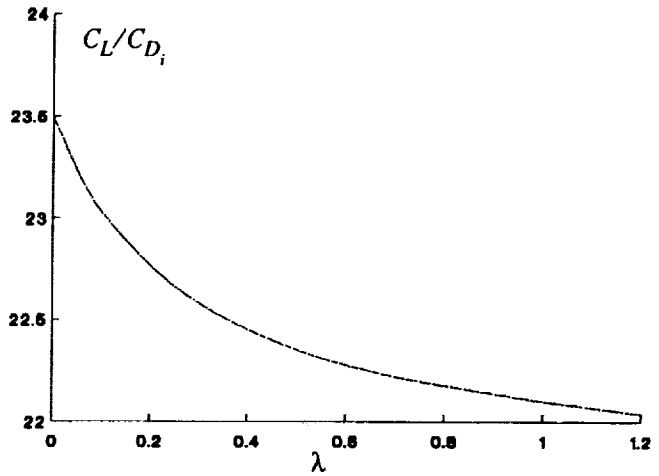


Fig. 23 Variation of C_L/C_{D_i} with taper ratio, λ , for an elliptic blade.

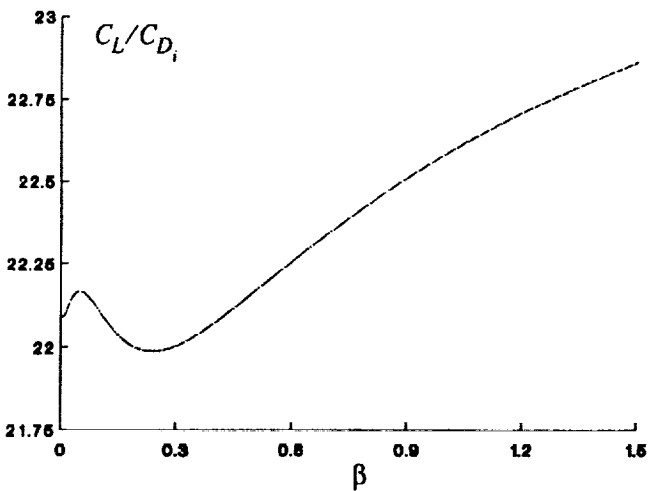


Fig. 21 Variation of C_L/C_{D_i} with tip length parameter, β , for an elliptic blade.

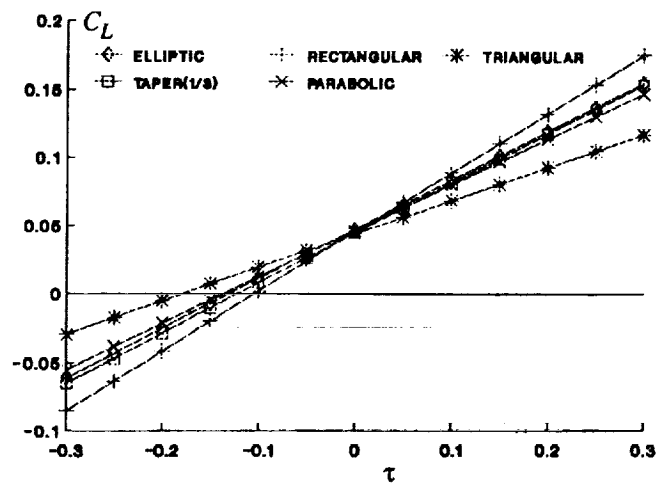


Fig. 24 Variation of C_L with twist ratio, τ , for various blade shapes.

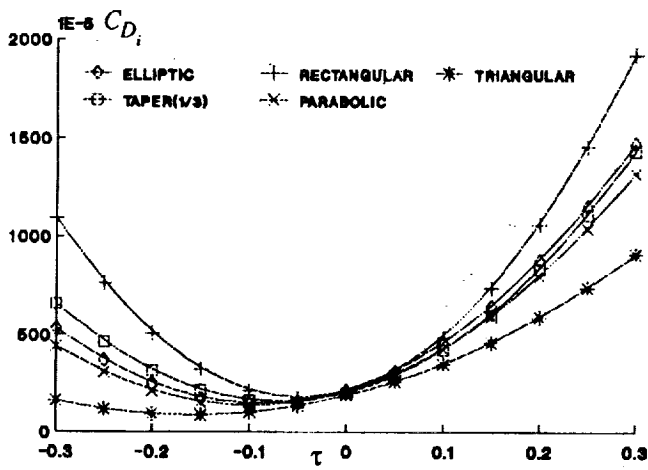


Fig. 25 Variation of C_{D_i} with twist ratio, τ , for various blade shapes.

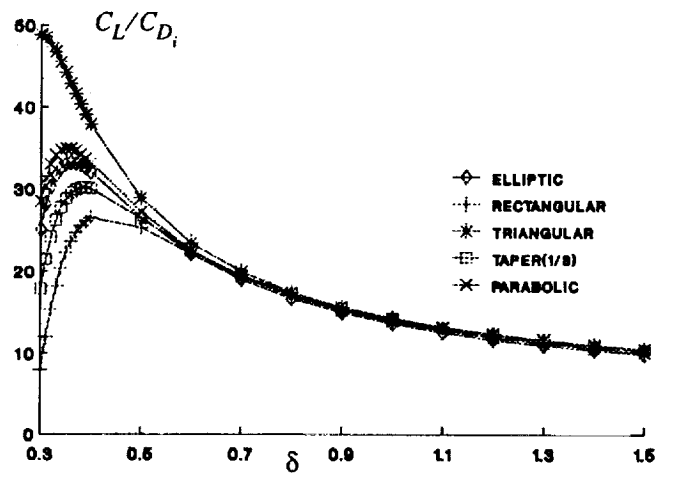


Fig. 27 Variation of C_L/C_{D_i} with twist shape parameter, δ , for various blade shapes.

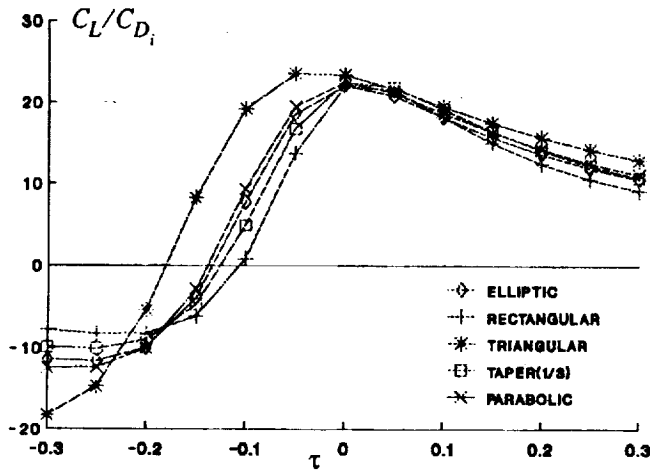


Fig. 26 Variation of C_L/C_{D_i} with twist ratio, τ , for various blade shapes.



Report Documentation Page

1. Report No. NASA CR-187524		2. Government Accession No.		3. Recipient's Catalog No.	
4. Title and Subtitle Aerodynamic Parametric Studies and Sensitivity Analysis for Rotor Blades in Axial Flight				5. Report Date March 1991	
				6. Performing Organization Code	
7. Author(s) Y. Danny Chiu David A. Peters				8. Performing Organization Report No.	
				10. Work Unit No. 505-63-36-06	
9. Performing Organization Name and Address Lockheed Engineering & Sciences Company Hampton, VA 23666 and Georgia Institute of Technology Atlanta, GA 30332				11. Contract or Grant No. NAS1-19000 NAG1-710	
				13. Type of Report and Period Covered Contractor Report	
12. Sponsoring Agency Name and Address National Aeronautics and Space Administration Langley Research Center Hampton, VA 23665-5225				14. Sponsoring Agency Code	
				15. Supplementary Notes Y. Danny Chiu: Lockheed Engineering & Sciences Company, Hampton, VA David A. Peters: Georgia Institute of Technology, Atlanta, GA Presented at the International Technical Specialists' Meeting on Rotorcraft Basic Research, Atlanta, GA March 25-27, 1991. Technical Monitor-H. M. Adelman	
16. Abstract <p>This paper offers analytical capability for aerodynamic parametric studies and sensitivity analyses of rotary wings in axial flight by using a 3-dimensional undistorted wake model in curved lifting-line theory. The governing equations are solved by both the Multhopp Interpolation technique and the Vortex Lattice method. The singularity from the bound vortices is eliminated through the Hadamard's finite part concept. Good numerical agreement between both analytical methods and finite differences methods are found. Parametric studies were made to assess the effects of several shape variables on aerodynamic loads. It is found, for example, that a rotor blade with out-of-plane and inplane curvature can theoretically increase lift in the inboard and outboard regions respectively without introducing an additional induced drag.</p>					
17. Key Words (Suggested by Author(s)) Rotor blade, Aerodynamics, Parametric Study, Sensitivity Analysis			18. Distribution Statement Unclassified - Unlimited Subject Category - 02		
19. Security Classif. (of this report) Unclassified		20. Security Classif. (of this page) Unclassified		21. No. of pages 16	22. Price A03

